JOURNAL OF PROPULSION AND POWER
Vol. 19, No. 2, March–April 2003

Two-Phase Computational Fluid Dynamics Analysis Applied to Prefilming Pure-Airblast Atomizer

Philip E. O. Buelow,* Chien-Pei Mao,† Steven Smith,‡ and David Bretz§
Goodrich Corporation, West Des Moines, Iowa 50265

A portion of an effort to effectively integrate two-phase, three-dimensional computational fluid dynamics (CFD) analyses into the design process for fuel atomizers is presented. The primary focus is to assess the utility of using two-phase CFD analyses to guide effectively the design process for the fuel swirler and prefilmer for a pure-airblast atomizer. The study is limited to analysis of the fuel flow under conditions where there is no air pressure drop across the nozzle. Breakup of the liquid sheet is not addressed. Items of interest are 1) film thickness and its circumferential variation at the exit of the prefilmer, 2) velocity components of the fuel film at the exit of the prefilmer, 3) spray-cone angle, and 4) leading-edge fuel recirculation/backflow. The Fluent version 5.5 CFD package is used for all analyses. Two-phase flow is modeled using Fluent's implementation of the volume-of-fluid method. Computational results are presented for a baseline experimental fuel swirler that backflows fuel through the inner-air circuit and a modified geometry, guided by CFD, that all but eliminates the backflowing. The CFD results compare favorably with experimental data of film velocity, film thickness, spray-cone angle, and leading-edge recirculation/backflow.

Introduction

COMPUTATIONAL fluid dynamics (CFD) analysis plays a valuable role in the fuel injector design process for both aerospace and industrial gas turbines. It is used to give insight into the design that cannot otherwise be obtained or that would be more costly and time-consuming to obtain by other means. Single-phase CFD analyses are commonly used in the gas turbine fuel nozzle design process of the air, gaseous fuel, and internal liquid fuel circuits. These applications of CFD have proved to be very successful in identifying and rectifying potential weaknesses in the designs. The situation is different when it comes to the actual liquid fuel atomization process, where there is a two-phase interaction between the liquid fuel and air. In this case, one must turn to experimental analyses and rely upon past experience, "cut-and-try" methodology, and design of experiments. Whereas these methods have yielded successful designs, it is preferable to have an analytical tool to gain insight into how and why geometry changes influence performance and give guidance to the design process.

Because multiphase CFD techniques have matured and available computing power has increased, the possibility now exists that multiphase CFD analysis can be integrated into the design process for practical hardware, not just large-scale research models. Steinthorsson and Lee[1] have demonstrated the application of two-phase CFD analysis to simulate the internal flow of a large-scale pressure-swirl (simplex) atomizer and compared their results with the experimental findings of Wang et al.[2] Although the CFD results showed some discrepancies with the experimental results, much of the analysis compared well with experiment. Film thickness and velocity profiles at the tip of the injector compared favorably with the experimental results. In this paper, a two-phase, volume-of-fluid (VOF) technique[3] is used to simulate the flow through the fuel swirler and the prefilmer of a pure-airblast atomizer under static conditions, that is, no air pressure drop across the nozzle. Effective atomization for a pure-airblast atomizer is predicated on the presentation of a thin, uniform film of fluid on a prefilming surface, which is then atomized by high-velocity air. The primary focus of the analysis will be on the internal flow characteristics of the fuel swirler, the formation of the liquid film on the prefilmer, and the resulting cone angle. No attempt is made to model the atomization of the liquid film.

The experimental fuel swirler analyzed in this study is characterized by a condition where the fuel exiting the annular spin chamber splits into two streams: one that flows downstream to form the conical liquid sheet and another that flows upstream through the inner air circuit. This condition is only present under static conditions. Under normal operating conditions, that is, positive air pressure drop across the nozzle, all of the fuel exits downstream to form a conical liquid sheet. This fuel swirler was analyzed using CFD. Geometry modifications were made based on the CFD results to reduce or eliminate the backflowing. The modified fuel swirler was then analyzed at different fuel flow rates using CFD. Following the CFD analysis, the modified hardware was fabricated and tested in the laboratory and comparisons were made between the CFD and the experimental findings of leading-edge recirculation/backflow, film velocity, film thickness, and cone angle.

General Flowfield Description

Figure 1 shows a schematic of the tip geometry and flowfield for the fuel swirlers considered in this study, under conditions of no air pressure drop. Swirl is imparted to the fuel stream by the spin slots. The fuel then travels toward the tip through the fuel conic (or spin chamber). As the fuel exits the fuel conic, it has a high degree of swirl. Some or all of the fuel may travel downstream, across the fuel prefilmer, and fan out into a spray cone. In some cases, a portion of the fuel may turn and travel upstream (called backflowing). For all configurations examined in this study, the fluid was MIL-C-7024-Type II. The density, viscosity, and surface tension of this fluid at a standard temperature of 298 K are 765 kg/m^3, 0.00092 kg/m · s, and 0.0223 N/m, respectively. A cross section of the tip geometry and CFD solution domain for the baseline fuel swirler/prefilmer is shown in Fig. 2. Because there are only three spin slots to the fuel swirler, we take advantage of the symmetry and solve for a 120-deg sector, to reduce the size of the mesh.

The full CFD solution domain is shown in Fig. 3, along with the indicated boundary conditions. The boundary condition at the fuel

Presented as Paper 2001-3938 at the AIAA/ASME/SAE/ASEE 37th Joint Propulsion Conference, Salt Lake City, UT, 8–11 July 2001; received 18 June 2002; revision received 25 November 2002; accepted for publication 26 November 2002.

*Senior Design Engineer, Turbine Fuel Technologies, 811 4th Street. Senior Member AIAA.
†Director of Research, Turbine Fuel Technologies, 811 4th Street.
‡Engineering Manager, Thermal Fluids, Turbine Fuel Technologies, 811 4th Street. Senior Member AIAA.
§Senior Engineering Technologist, Turbine Fuel Technologies, 811 4th Street.

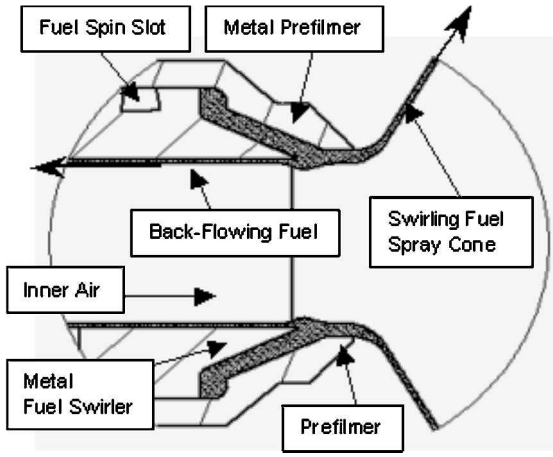

Fig. 1 Schematic of cross-section of tip of fuel swirler/prefilmer, showing possible fuel flow paths, and spray cone.

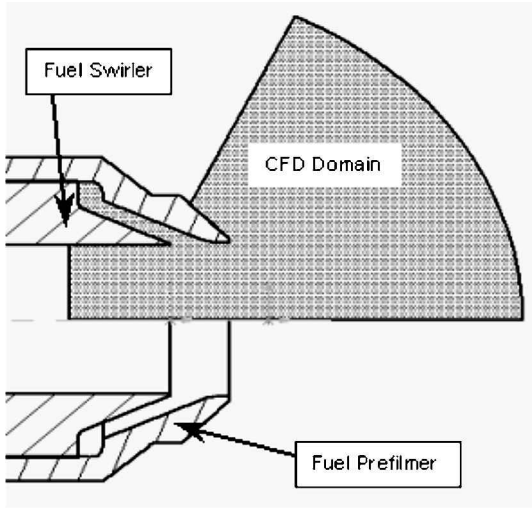

Fig. 2 Cross section of the baseline fuel swirler and CFD solution domain.

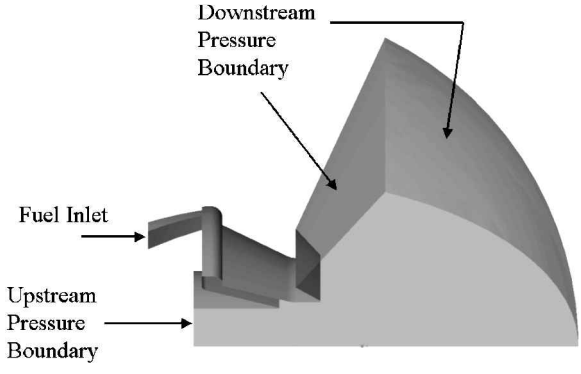

Fig. 3 Full CFD solution domain (120-deg sector) showing inflow and outflow boundaries; planar sides are periodic boundaries.

inlet was a specified velocity normal to the boundary. The magnitude of the velocity was determined by the mass flow rate for the case, which was specified at 0.00505, 0.00758, or 0.0139 kg/s for the full nozzle, that is, all three slots combined. These three flow rates are equivalent to 40, 60, and 110 lb/h. The Reynolds number for the highest flow rate was 1×10^5 based on the velocity at the exit of the spin slot, the density and viscosity of the fluid medium, and the diameter of the prefilmer. The fuel inlet flow was assumed turbulent with a 10% turbulence intensity. The upstream and downstream pressure boundaries were both set to ambient pressure (101325 N/m^2, 14.7 psia) for the static condition, that is, no air pressure drop. Rotationally periodic boundary conditions were specified on the two 120-deg planar boundaries. All wall boundaries were taken as no-slip.

Experimental data were also taken to compare with the CFD results. Axial and radial velocity components of the edge of the film were measured in the laboratory using Phase Doppler Particle Analyzer (PDPA) equipment. High-speed photographs were also taken of the liquid film near the exit of the atomizer to visualize the film and obtain spray cone angle measurements. All data were taken for static conditions, with no air pressure drop across the atomizer. Descriptions of the PDPA and high-speed photography procedures may be found by Mao.[4]

Numerical Solution Procedure

The numerical simulations in this study solve the incompressible Reynolds averaged Navier–Stokes equations along with a volume fraction (VOF) equation to determine the interface between the air and the liquid fuel. Many methods exist to simulate two-phase flowfields, and a cursory examination of the currently available techniques may be found by Steinthorsson and Lee.[1] We will not address the merits of these various techniques, but rather make judicious use of the one provided in the commercial software employed in our design process: the VOF method in Fluent version 5.5. Surface tension effects are modeled using the continuum surface force model of Brackbill et al.,[5] and gravity effects are not included in these analyses.

The volume fraction equation can be solved using standard upwind differencing techniques, which tend to smear the interface over a few cells, or by geometric reconstruction[6] of the two-phase interface, which ensures that the two-phase boundary is captured within one computational cell. In either case, a very fine grid is required in the vicinity of the two-phase boundary. The upwind differencing technique can be used with a steady-state solution procedure, whereas the geometric reconstruction technique must be used in conjunction with a time-accurate approach. Thus, performing two-phase, VOF simulations with geometric reconstruction can take an order of magnitude more CPU time than when using upwind differencing with a steady-state analysis. Because rapid turnaround is required in a design effort, we have chosen to employ the upwind differencing technique to simulate the two-phase boundary so that we can perform steady-state analyses, which can give us a 1-day turnaround as opposed to a 10–20 day turnaround for the time-accurate analysis.

The turbulent viscosity was determined by solving the Renormalization Group (RNG) k–epsilon two-equation model with either wall functions or the two-layer model of Wolfstein[7] (also Ref. 6). Modifications to the RNG model for swirling flows, as well as the differential viscosity model, were also employed. (See Ref. 6 for details).

The grid spacing necessary to model the two-phase interface resulted in near-wall $Y+$ values in the range $5 < Y+ < 40$, for the wall-function approach. This is just below the low end for wall functions, and it was hoped that the differential viscosity model for wall functions would help to compensate for the near-wall region being closer to the laminar sublayer region. To remove some of the uncertainty with wall functions, the two-layer turbulence model of Wolfstein[7] was also employed. For the two-layer model, the first $Y+$ value off the wall was maintained below unity (typically on the order of 0.1). The RNG form of the k–epsilon equations was solved because the flowfields encountered in fuel nozzles are typically highly swirling and the RNG model contains modifications for swirling flowfields.[6] However, it is known that the turbulence effects in highly swirling flowfields are generally poorly modeled by two-equation models, due to the high degree of anisotropy present in the turbulence fields. Even though this limitation exists, advanced two-equation turbulence models are commonly used to model the highly swirling flowfields of fuel atomizers and gas-turbine combustors, and reasonably good qualitative results are obtained.[8]

Another obvious concern for two-phase simulations is the ability to model correctly the turbulence in the presence of liquid and air. The issue of turbulence modeling in multiphase flows is beyond the scope of this paper and will not be addressed here. We are

investigating the use of the existing design tool (Fluent version 5.5) and its current models.

The governing system of equations is integrated using the Fluent version 5.5 package. The steady-state analysis is performed using the segregated solver with pressure–velocity coupling handled by the SIMPLE method. Spatial differencing is first-order upwind for the momentum and turbulence equations and second-order upwind for the volume fraction transport equation. The choice of first-order upwind differencing was to ensure a stable solution at the expense of some accuracy.

The grids for these analyses were generated using Fluent's grid generator, Gambit. The process of generating the grid consisted of first generating a solid representation of the CFD solution domain, called an "aerovolume" (Fig. 3), using a CAD program. The aerovolume was imported into the grid generator, where an unstructured hexahedral (or hybrid, tetrahedral/prismatic/hexahedral) grid was generated and boundary surfaces were "tagged" to identify them for boundary conditions. The mesh sizes examined in this study ranged from 800,000 to 1.74 million cells.

The CFD runs were performed on a Dell Precision 620 workstation with 2 GB of RAM and two Pentium III 1-GHz processors. The operating system was Windows 2000.

Baseline Configuration

The baseline configuration is an experimental swirler that was found to exhibit the undesirable feature of backflowing fuel upstream through the inner-air circuit under static conditions, that is, no air pressure drop. However, when there is a positive air pressure drop across the nozzle, all of the fuel exits downstream in a conical spray, which is the desired operation of the nozzle. The tip of the fuel swirler/prefilmer along with the CFD solution domain is shown in Fig. 2. Two grids were generated for this case. The grid used for the wall-function approach is an unstructured hexahedral grid consisting of approximately 900,000 cells. The grid used for the two-layer turbulence modeling approach is a hybrid unstructured grid with local prismatic/hexahedral grids tightly spaced near the walls to ensure that the $Y+$ values for the first grid cell off the wall are less than unity. This two-layer grid consists of approximately 1.3 million cells. The tetrahedral and prismatic cells are located in the fuel spin slot; the remaining cells are all hexahedral. Figure 4 shows a representative cross section of one of the grids, where it is evident that grid cells are locally concentrated in regions where the two-phase boundaries were determined (by coarse grid calculations) to be located. This case was run at a fuel flow rate of 0.00758 kg/s. Actual experimental hardware for this configuration was tested in the laboratory, and it was found that 23% ± 1% of the liquid backflowed.

The CFD results are presented in Fig. 5, which shows volume fraction contours at one cross section of the domain and a closeup of the tip showing velocity vectors. The fuel flow splits into a downstream flowpath, which forms the conical film, and an upstream flowpath along the wall of the inner air circuit, that is, backflowing. The reason for the backflowing is as follows. As the flow exits the fuel conic, there is inadequate frontal area for all of the flow to issue downstream in the axial direction. Therefore, a portion of the flow is forced radially inward as it exits the fuel conic to maintain mass conservation. Once the flow exits the fuel conic, it is free to travel either upstream or downstream depending on the balance of forces. The high degree of swirl in the flow causes it to move radially outward once again, and the flow is forced both upstream and downstream. Thus, the backflowing is due primarily to the dynamics of the highly swirling flow.

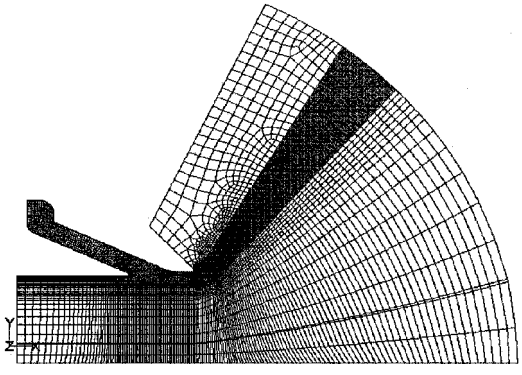

Fig. 4 Cross section of a grid for the baseline configuration; three-dimensional grid consists of 1.3 million cells.

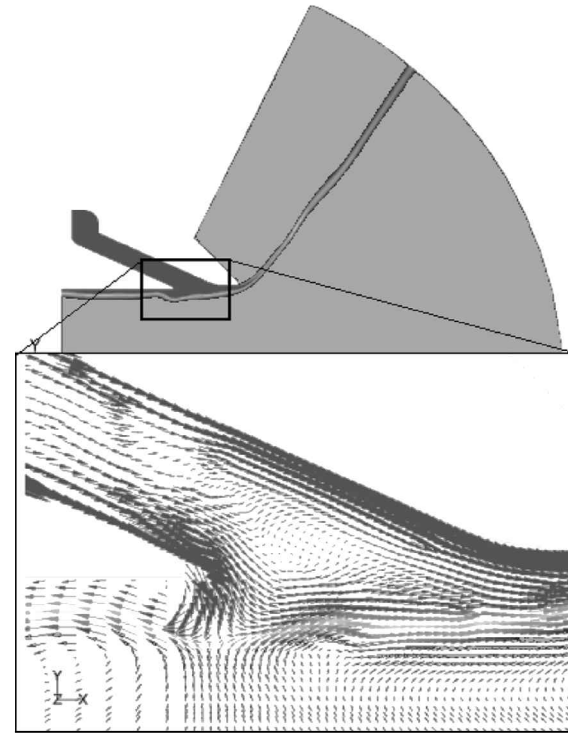

Fig. 5 Contours of liquid volume fraction for the baseline configuration at 0.00758 kg/s (60 lb/h), at a cross-section of the domain, with closeup of velocity vectors at the tip: dark gray, liquid and light gray, air.

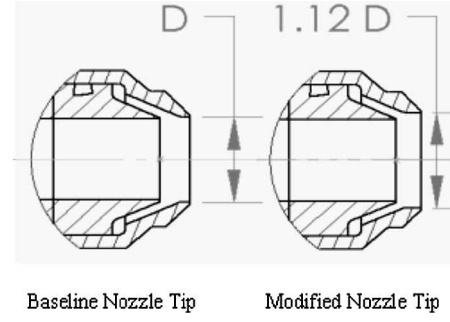

Fig. 6 Cross section of the tip of the fuel swirler/prefilmer for modified configuration, compared with the baseline. Note increase in diameter of the prefilmer on modified configuration.

The CFD results predict a 22% (by mass) backflowing of fuel under static conditions when using wall functions and a 26% backflowing when using the two-layer model. The predicted level of backflowing is in the range of that found from experiment and indicates that the CFD simulation is capturing this phenomenon. The spray angle was predicted to be 108 deg, which was about 9% below the measured value of 118 deg.

Because the intention of this study is to assess the utility of two-phase CFD modeling in the design process, a modification was made to the baseline configuration with the intent of reducing or eliminating the backflowing. This modification was first analyzed using CFD and then was tested in the laboratory to verify the CFD predictions. The design modification was to increase the diameter of the prefilmer to promote a more significant downstream axial flow exiting the spin chamber. The resulting geometry is shown in Fig. 6.

Modified Configuration

Backflowing

The modified configuration was studied more extensively than the baseline. An initial CFD run at 0.00758 kg/s was performed to see if the backflowing was alleviated. Indeed, no backflowing was observed when the wall-function approach (for turbulence modeling) was used. However, when the two-layer turbulence modeling approach was employed, a slight amount (less than 0.5%) of backflowing was predicted (Fig. 7). This slight amount of backflowing predicted by the two-layer model was in fact observed in the laboratory experiments of the modified configuration.

Figure 7 shows contours of the volume fraction on a cross section of the atomizer for both the wall-function and two-layer approachs. As seen in Fig. 7b, there is a small amount of liquid along the wall of the inner-air circuit upstream of the prefilmer. The difference in the two predictions is due to the resolution of the near-wall region at the exit of the spin chamber (Fig. 8).

As seen in Fig. 8, the two-layer model resolves the low-momentum boundary layer, where liquid is able to pass around the lip and progress upstream. The liquid is able to flow upstream because there is no pressure gradient driving air through the inner-air circuit to counteract the hydraulic phenomenon. If there were a typical favorable pressure gradient through the inner-air circuit, there would be sufficient air momentum to prevent any backflowing. There is a minor flow of air through the inner-air circuit induced by "viscous-pumping" caused by the liquid flow. Also Fig. 8 shows the inability of the wall-function approach to capture this low-momentum region, due to the coarser grid, resulting in no predicted backflowing.

CFD simulations were then run at 0.00505, 0.00758, and 0.0139 kg/s (40, 60, 110 lb/h) using only the two-layer model because of its ability to capture the small amount of backflowing. Comparisons of the CFD results were made with data taken from laboratory experiments of the modified configuration.

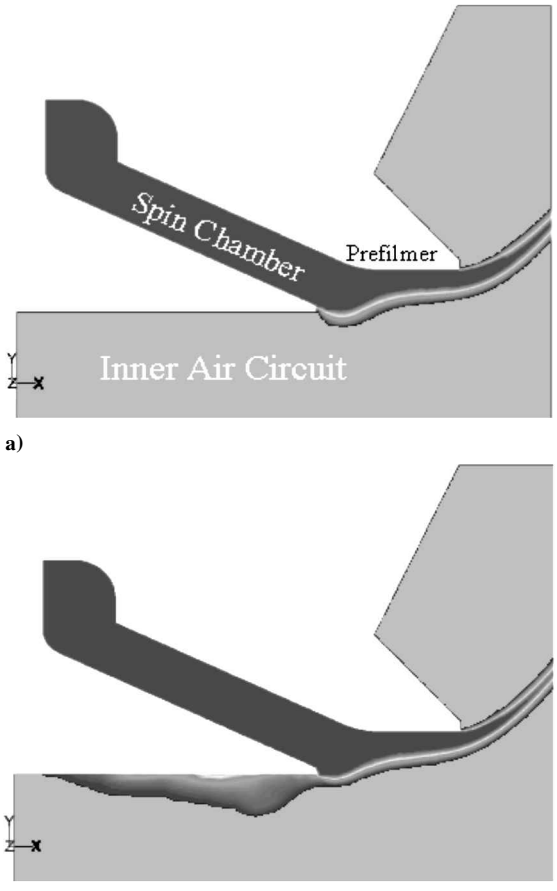

Fig. 7 Contours of liquid volume fraction (dark gray) at cross section of domain for modified configuration; fuel flow = 0.00758 kg/s: a) wall-function model and b) two-layer model.

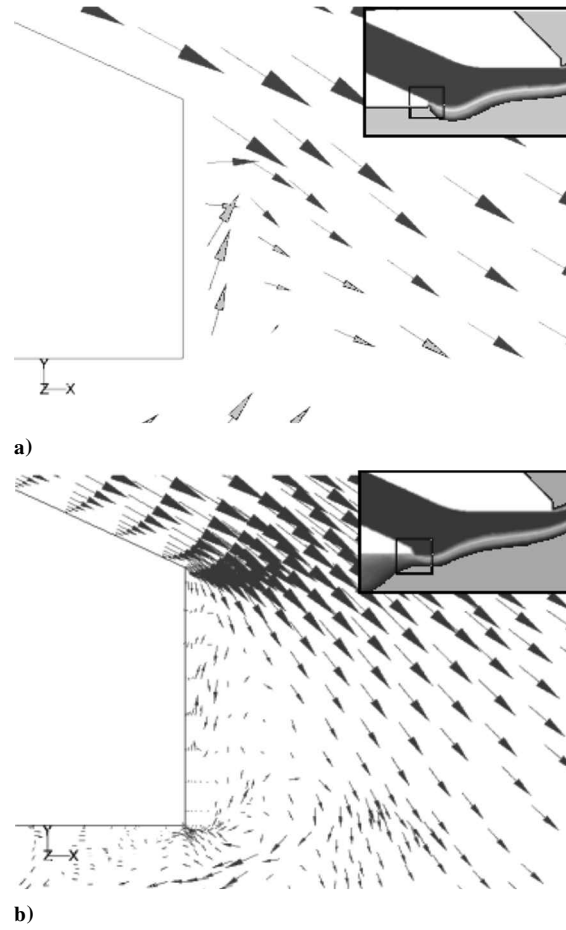

Fig. 8 Velocity vectors at the exit of the fuel conic (insets) showing flowfield resolution between a) wall-function model and b) two-layer model.

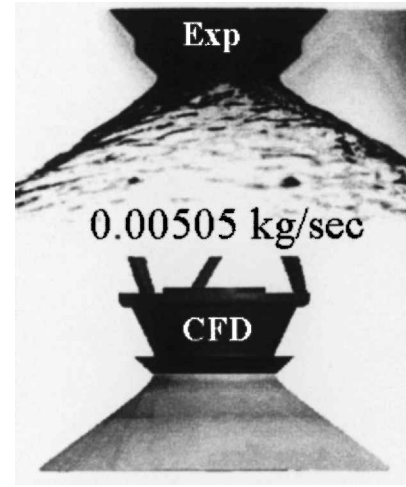

Fig. 9 Comparison of cone angle between experiment (117 deg) and CFD (107 deg) at 0.00505 kg/s (40 lb/h).

Cone Angle Comparison

The liquid film cones exiting from the atomizer for each of the three cases (0.00505, 0.00758, and 0.0139 kg/s) are compared with photographs from the laboratory experiments in Figs. 9–11, respectively. Cone angles were measured from both the photographs and

Table 1 Comparison of axial and radial velocity components for the 0.00505-kg/s (40 lb/h) case

	Axial velocity, m/s				Radial velocity, m/s			
Axial distance, mm	CFD	Experiment	Standard deviation	% Difference	CFD	Experiment	Standard deviation	% Difference
0	1.7	——	——	——	0.4	——	——	——
1	1.7	1.45	1.00	16.4	2.1	2.72	1.34	−22.8
2	1.8	1.53	0.62	17.6	2.3	2.90	0.8	−20.7
3	1.8	1.59	0.66	13.2	2.4	3.02	0.76	−19.9
4	1.8	1.64	0.54	9.8	2.3	3.01	0.66	−23.6

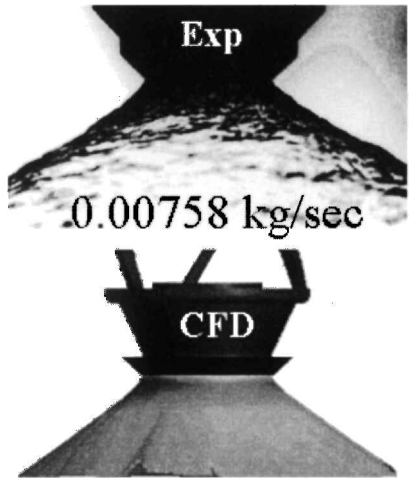

Fig. 10 Comparison of cone angle between experiment (118 deg) and CFD (108 deg) at 0.00758 kg/s (60 lb/h).

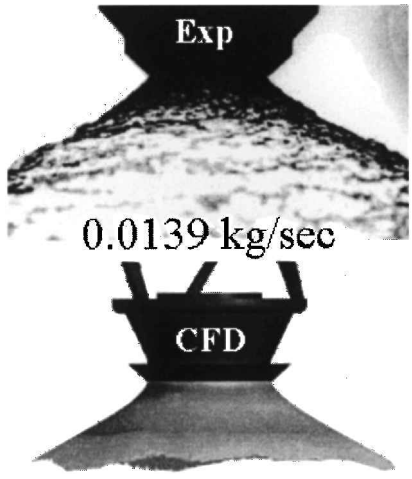

Fig. 11 Comparison of cone angle between experiment (128 deg) and CFD (121 deg) at 0.0139 kg/s (110 lb/h).

the CFD results by drawing tangents to the film surface at approximately 4 mm downstream from the tip and measuring the included angle between these two tangents. Within 10 mm of the tip of the nozzle, the fuel remains as a coherent sheet of liquid and does not atomize until after approximately 15–30 mm from the tip, depending on the flow rate.

Similar to the baseline configuration, predicted cone angles were smaller than the experimental results. The 0.00505- and 0.00758-kg/s cases underpredicted the cone angle by approximately 9%, and the 0.0139-kg/s case underpredicted the cone angle by about 5%. The effect of the near-wall model (wall-function model vs two-layer model) had a negligible effect on the predicted cone angles. This underprediction of cone angle is consistent with other CFD results.[1]

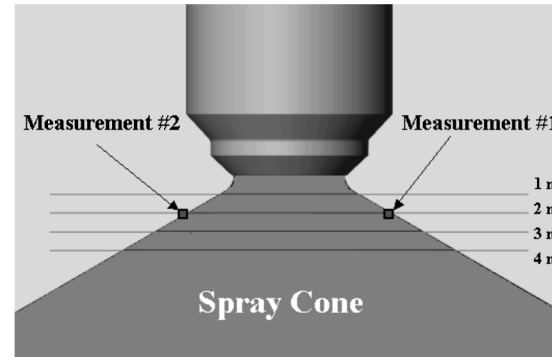

Fig. 12 Locations along the spray cone where the PDPA data were taken.

Film Velocity Comparison

Axial and radial velocity components for each of the three cases were also compared. Tangential velocities were not directly measured experimentally; therefore, no comparison was made for the tangential velocity components. However, the effect of the tangential velocities is manifest in the extent of the spray cone angle, which is underpredicted by the CFD simulations. This indicates that the CFD results may be underpredicting the magnitude of tangential velocities.

The experimental values of velocity components were obtained using the PDPA equipment. Approximately 3000 PDPA samples were taken for each value of velocity. Measurements were taken at 1, 2, 3, and 4 mm downstream from the exit of the prefilmer. At each axial location, two measurements were taken in a plane that bisects the spray. One measurement was taken at one edge of the spray and the other at the opposing edge (Fig. 12). The experimental sprays were skewed relative to the centerline of the nozzle (maximum deviation of ~10 deg), which indicates that the two components that make up the atomizer were not in perfect alignment. To compare the experimental data with the CFD results, the two measurements (at each axial station) were averaged, and this averaged value was compared with the CFD results.

The comparison of axial and radial velocity components for the 0.00505-kg/s case is given in Table 1. Because the predicted cone angle is shallower than the measured cone angle, it is expected that the axial component of velocity will be overpredicted and that the radial component of velocity will be underpredicted. This is indeed the case as seen from the tabulated results. Predicted values of velocity components differ from the mean of the experimentally measured values by 8–25%. The standard deviation of the experimental values is also reported in Table 1 and gives an indication of the spread in the measurements. To assess the relative quality of the experimental data between the three cases, one can compare the coefficients of variation (CV) equal to standard deviation divided by the mean. A smaller value of CV would indicate a smaller spread in the experimental data. If the CV is calculated for each of the three cases, it is evident that the spread in experimental data is reduced for the higher flow rates. This suggests that the quality of the experimental data is better at the higher mass flow rates.

Tables 2 and 3 show the axial and radial velocity comparisons for the 0.00758- and 0.0139-kg/s cases, respectively. The same trends are seen as for the 0.00505-kg/s case. However, the 0.0139-kg/s case appears to give the closest comparison with the experimental data.

Table 2 Comparison of axial and radial velocity components for the 0.00758-kg/s (60 lb/h) case

	Axial velocity, m/s				Radial velocity, m/s			
Axial distance, mm	CFD	Experiment	Standard deviation	% Difference	CFD	Experiment	Standard deviation	% Difference
0	2.8	——	——	——	0.6	——	——	——
1	2.8	2.69	1.09	4.1	3.6	4.17	1.53	−13.7
2	3.1	2.77	1.01	11.9	4.4	4.69	1.24	−6.2
3	3.4	2.75	0.83	23.6	4.6	4.88	1.13	−5.7
4	3.5	2.64	0.85	32.6	4.8	5.23	0.86	−8.2

Table 3 Comparison of axial and radial velocity components for the 0.0139-kg/s (110 lb/h) case

	Axial velocity, m/s				Radial velocity, m/s			
Axial distance, mm	CFD	Experiment	Standard deviation	% Difference	CFD	Experiment	Standard deviation	% Difference
0	5.3	——	——	——	1.0	——	——	——
1	5.4	5.43	1.52	−0.6	6.9	8.73	2.18	−21.0
2	5.5	5.50	1.17	0.0	8.9	10.14	1.82	−12.2
3	5.6	6.40	1.00	1.9	9.7	10.64	1.44	−8.8
4	5.6	5.39	1.16	3.9	9.9	10.63	1.42	−6.9

Table 4 Comparison of film thickness at 0, 1, 2 mm downstream from prefilmer exit for 0.00505-, 0.00758-, and 0.0139-kg/s flow rates

	Film thickness, μm		
Axial distance, mm	CFD	Experiment	% Difference
	0.00505 kg/s		
0	231	259.5	−11.0
1	84	87.9	−4.4
2	77	54.1	42.3
	0.00758 kg/s		
0	192	216.9	−11.5
1	81	82.0	−1.2
2	67	52.4	27.9
	0.0139 kg/s		
0	185	194.3	−4.8
1	67	64.5	3.9
2	45	40.9	10.0

Table 5 Predicted values of patternation and SUI as measures of circumferential nonuniformity in fuel flow at the exit of prefilmer

Measure	0.00505 kg/s (40 lb/h)	0.00758 kg/s (60 lb/h)	0.0139 kg/s (110 lb/h)
Patternation	18.9	14.93	13.44
SUI	6.95	5.6	4.93

Film Thickness Comparison

The thickness of the liquid film at the exit of the prefilmer, as well as the downstream variation of film thickness, is also of interest. Because the film thickness cannot be measured directly in the laboratory, it is derived from the mass flow constraint, local velocity measurements, radial location of the edge of the film, and the measured cone angle, along with the assumption of an axisymmetric cone. Further assumptions have to be made to estimate the film thickness at the exit plane of the prefilmer because film velocities cannot be directly measured at this location. These further assumptions are that the axial velocity at the exit of the prefilmer is equal to the axial velocity at the 1-mm measurement location and that the radial component of velocity is 0 m/s. The first assumption for axial velocity is justified by observing from Tables 1–3 that the axial component of velocity does not change appreciably in the near field as the film progresses downstream. The second assumption of zero radial velocity at the exit of the prefilmer arises from the geometric constraint of the prefilmer.

Because the film thickness decreases with downstream axial distance, the grid density for the CFD runs was insufficient to resolve the liquid film beyond the 2-mm measurement location. Downstream of the 2-mm location, the film thickness was on the order of 1–2 grid cells (even with 1.3 million cells in the computational domain).

Comparisons of the film thickness are presented in Table 4 for the 0.00505-, 0.00758-, and 0.0139-kg/s cases, respectively. For the CFD results, the air–liquid interface (edge of the film) was taken to be the location where the volume fraction equals 0.5.

It is evident from Table 4 that the average film thickness determined from experimental data decreases as the fuel flow rate is increased, and the CFD results correctly capture this trend. The differences in film thickness between the CFD results and the experimentally derived values are within 12% for all three cases up to the 1-mm axial location. At 2 mm and beyond, the grid density is insufficient to make any reasonable comparisons. However, the predicted value of film thickness at 2 mm is included in Table 4 to show the marked reduction in accuracy at the 2-mm location. Again, the 0.0139-kg/s case appears to yield the closest overall comparison with experiment.

Circumferential Fuel Distribution

Finally, an examination of the circumferential variation of the fuel distribution at the exit plane of the prefilmer is presented. No experimental data are available for this metric, so only CFD data will be presented. In this study, we present two measures of circumferential nonuniformity: 1) patternation and 2) spray uniformity index (SUI).[9] Both of these indices require dividing the exit plane of the prefilmer into a finite number of circumferential sectors. In this case, we divide our 120-deg domain into 12 sectors of 10 deg each. The patternation is determined by taking the difference between the sectors with the maximum and minimum mass flow rates of liquid and dividing by the average of all of the sectors:

$$\text{patternation} = (\dot{m}_{\max} - \dot{m}_{\min})/\dot{m}_{\text{av}} \times 100\%$$

The SUI is simply a standard deviation of the mass flow rate through each of the sectors and is given by

$$SUI = \sqrt{\sum_{s=1}^{N}\left(W_s - \frac{100}{N}\right)^2 \Bigg/ (N-1) \times N}$$

where W_s is the percent mass flow rate of liquid through any given sector and N is equal to the number of sectors. (In this case it would be equal to 12.) Table 5 shows the values of predicted patternation and SUI for the three fuel flow rates examined in this study. Without experimental data, it is difficult to determine the veracity of the

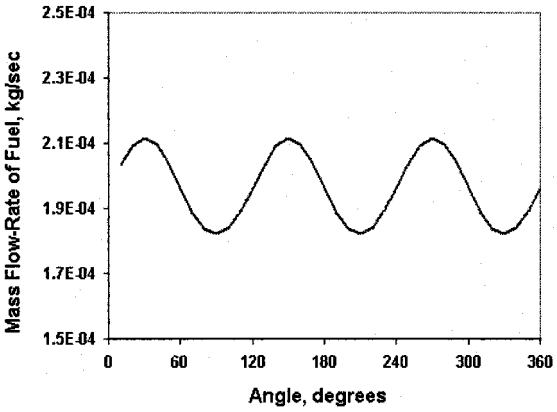

Fig. 13 Circumferential variation of liquid mass flow rate at the exit of the prefilmer for the two-layer model at 0.00758 kg/s (60 lb/h).

results. However, a circumferential variation in mass flow rate is predicted, as shown in Fig. 13 for the 0.00758-kg/s case, and it corresponds to the number of fuel spin slots (3 spin slots per 360 deg, which produces 3 wavelengths per 360 deg).

Grid-Refinement Study

To assess any possible changes in the solution due to further refinement of the grid, a brief grid-refinement study was performed for the 0.00758-kg/s case. The total number of cells was increased from 1.17 million to 1.74 million, with a localized doubling of the number of cells on the subvolume that contains the conical liquid sheet. Results indicated that the spray-cone angle remained unchanged, and that the circumferential patternation increased to 17%. The film thickness at the exit of the prefilmer increased and is now only 3% less than the experimentally derived value. The predicted velocity components changed by no more than 4%. These results indicate that the solution is not yet grid independent; however, the trend is toward closer comparison with the experimental data.

At this level of refinement, the residuals are starting to show signs of unsteadiness (although the flow variables appear steady), which suggests that any further refinement of the grid will likely lead to unsteady flow features that will require time-accurate modeling. Because the character of these flowfields is naturally unsteady, sufficient grid refinement will lead to a modeling resolution that will be able to capture the inherent flow instabilities leading to unsteadiness. The current level of grid resolution still provides enough artificial dissipation to damp out those flow instabilities.

Summary

The applicability of two-phase CFD modeling to the design process has been investigated using current design tools (in this case the VOF model in Fluent version 5.5). The application was the modeling of the fuel swirler and prefilmer of an experimental pure-airblast atomizer under static conditions, that is, no air pressure drop across the nozzle. The baseline nozzle had the undesirable characteristic of backflowing fuel upstream through the inner-air circuit under static conditions. A design modification, based on CFD modeling, was made to alleviate the backflowing of fuel through the inner-air circuit. The flow characteristics of cone angle, film velocities, film thickness, and circumferential nonuniformity were assessed using CFD, followed by experimental measurements in the laboratory using PDPA equipment and high-speed photography. Given that rapid turnaround times are required for effective design cycle times, low-order steady-state CFD analyses were employed in this study. The turnaround time from solid model to mesh to CFD solution was 1 day, where the CFD run was performed overnight. Comparisons of the CFD results with the experimental data were found to be acceptable for qualitative assessment of a design or design modifications. Good quantitative accuracy will most likely require higher-order, time-accurate CFD analyses, which is currently beyond the constraints of our design cycle times.

To extend the analysis to a full 360-deg model to capture flow variations through each of the spin slots, the number of grid cells would have to be tripled (to 4 million cells) just to maintain the same resolution as the current study. To extend this type of analysis further to include the interaction of high-velocity air with the liquid fuel sheet (to model pure-airblast operation at engine conditions), even finer grid resolution would be required to capture the prompt atomization near the tip of the nozzle, the dispersion of the resulting spray field, and the air–velocity field. This level of analysis would most likely require on the order of 100 million cells, and require at least a large-eddy simulation, which by nature is unsteady. All of this is just to model the near-field two-phase atomization process (5–10 mm from the tip of the nozzle). To make this level of analysis tractable for design purposes, a massively parallel processing architecture would be required to meet the goal of a 1-day turnaround time.

References

[1]Steinthorsson, E., and Lee, D., "Numerical Simulations of Internal Flow in a Simplex Atomizer," *Proceedings of the Eighth International Conference on Liquid Atomization and Spray Systems*, Pasadena, California, July 2000.

[2]Wang, D., Ma, Z., Jeng, S.-M., and Benjamin, M. A., "Internal Flow Structure of a Pressure-Swirl Atomizer at Two Different Density Ratios," American Society of Mechanical Engineers, Paper ASME 2000-GT-119, Munich, Germany, May 2000.

[3]Hirt, C. W., and Nichols, B. D., "Volume of Fluid Method for the Dynamics of Free Boundaries," *Journal of Computational Physics*, Vol. 39, 1981, pp. 201–225.

[4]Mao, C.-P., "The Dynamics of a Swirling Liquid Film," *Proceedings of the Eighth International Conference on Liquid Atomization and Spray Systems*, Pasadena, California, July 2000.

[5]Brackbill, J. U., Kothe, D. B., and Zemach, C., "A Continuum Method for Modeling Surface Tension," *Journal of Computational Physics*, Vol. 100, 1992, pp. 335–354.

[6]"Fluents User's Guide," Vol. 1–4, Fluent, Inc., Lebanon, NH, 1998.

[7]Wolfstein, M., "The Velocity and Temperature Distribution of One-Dimensional Flow with Turbulence Augmentation and Pressure Gradient," *International Journal of Heat and Mass Transfer*, Vol. 12, 1969, pp. 301–318.

[8]Mongia, H. C., "Combustion Modeling in Design Process: Applications and Future Direction," AIAA Paper 94-0466, Jan. 1994.

[9]Deljouravesh, R., "An Optical Patternator for Quantitative and On-Line Spray Diagnostics," M.S. Thesis, Dept. of Mechanical Engineering, Queen's Univ., Kingston, ON, Canada, Oct. 1997.